Current Source Inverter-Fed Variable Reluctance Motor Drive with DC-Machine-Like Control Characteristics

Spasoje Mirić[1], Predrag Pejović[2], Michael Haider, and Takanobu Ohno[1]
[1] Drives and Energy Systems Laboratory, University of Innsbruck, 6020 Innsbruck, Austria
[2] School of Electrical Engineering, University of Belgrade, 11120 Belgrade, Serbia
Email: spasoje.miric@uibk.ac.at

***Abstract*—Variable reluctance motor (VRM) drives have been a subject of research for many years due to their simple construction and the ability to operate with unipolar phase currents, which simplifies inverter design. As a result, numerous inverter topologies tailored for VRMs have been proposed in the literature. However, irrespective of the chosen topology, the challenge of controlling the VRM phase currents remains. To relieve the user of the burden of managing VRM current control, this paper proposes a current source inverter (CSI)-supplied VRM drive system, where the CSI operates in open loop using only rotor position information, without requiring any user interaction. This approach allows the complete drive system to emulate the behavior of a series-excited DC machine from the CSI's DC side, enabling straightforward operation. A DC-side equivalent speed-torque characteristic is derived to support this concept, and simulation results are presented to validate the proposed approach.**

***Index Terms*—Switched reluctance machines, Variable reluctance machines, Current source inverters, Series-excited DC machine, Unipolar current drive, Inverter integration, Open-end winding**

I. Introduction

Variable speed drive (VSD) systems based on variable reluctance motors (VRMs), also commonly referred to as switched reluctance motors (SRMs), have attracted research interest for more than 55 years [1] due to their simple and robust construction. VRMs feature salient poles on both the stator and rotor, hence often referred to as doubly salient machines. They utilize concentrated windings on the stator with a simple construction, while the rotor contains neither windings nor permanent magnets. Torque is generated through the magnetic attraction between stator and rotor poles, with stator currents being switched on and off according to the rotor position [2], [3].

This switching process, where current is commutated from one coil to another, is challenging due to the large energies involved. As a result, significant research efforts have been dedicated to developing suitable inverter topologies, often tailored to specific VRM winding configurations, such as short-pitched or fully pitched windings [4], [5]. The currents in VRMs are unipolar, which enables simpler inverter topologies compared to those required for bipolar current operation. As a result, numerous publications have focused on developing simplified VRM inverter configurations aimed at minimizing the number of semiconductor devices per phase [6]–[9].

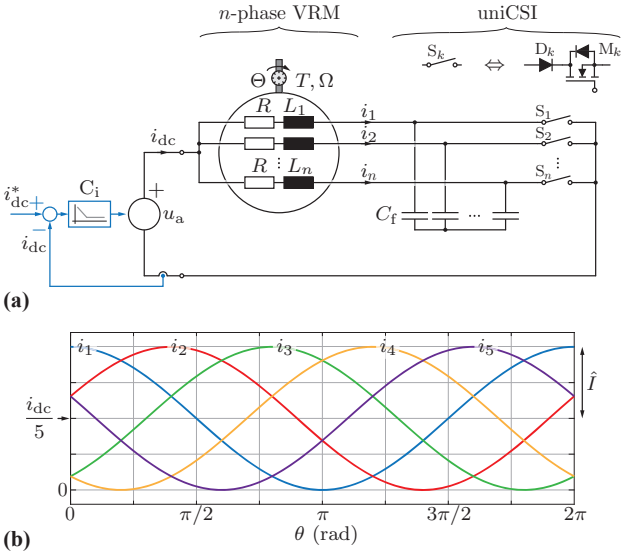

Fig. 1: (a) An n-phase VRM utilizing the switch-per-phase CSI configuration proposed in [10], so-called uniCSI. The need for a dedicated DC-link inductor is eliminated, as the inductance of the open-end winding SRM inherently facilitates CSI operation. **(b)** Unipolar VRM five-phase current waveforms, showing that phase currents remain strictly positive. θ is the electrical angle.

When VRM currents are switched off, the associated energy accumulated in the VRMs inductance is either dissipated in an external resistor or Zener diode, or returned to the power supply, each of which introduces various challenges. To mitigate these issues, a VRM with an additional winding was proposed in [11], improving turn-off performance by enabling internal energy circulation within the machine itself. Subsequently, VRMs featuring both AC and DC excitation windings were developed [12], [13], paving the way for designs that use a single set of windings to carry both AC and DC current components [14]–[16]. In such configurations, the VRM phase currents become unipolar sinusoidal (see **Fig. 1(b)**) rather than pulsed on/off waveforms, which significantly simplifies the control strategy. A recent wave of research has focused on inverter topologies capable of delivering high-frequency PWM voltages to VRMs in order to generate unipolar sinusoidal phase currents. Since these unipolar

currents do not sum to zero, forming a star point is not feasible. As a result, specialized inverter configurations such as full-bridge inverters per phase [17] or four-leg inverters [18], [19] are employed to accommodate this constraint.

Despite significant progress in VRM research and inverter development, there is still no standardized VRM inverter solution. This lack of standardization, along with non-standard control strategies, continues to hinder the widespread adoption of VRM-based drive systems. To address this, the present paper proposes a concept in which the user has no direct interaction with the VRM inverter. Instead, the VRM and its inverter are designed to behave as a single integrated unit, functionally equivalent to a series-excited DC machine. The inverter topology enabling this approach is a current source inverter (CSI) designed for unipolar currents, referred to as *uniCSI*. It requires only one switch per phase and operates without a DC-link inductor (see **Fig. 1(a)**), as proposed in [10]. In this paper, we demonstrate the operation of the proposed uniCSI-supplied VRM concept and establish its equivalence to a series-excited DC machine, using a fundamental-wave VRM model and sinusoidal phase currents with a DC offset, like those shown in **Fig. 1(b)**.

II. VRM Currents and uniCSI Duty Cycles

Torque generation in VRMs is traditionally described as the result of magnetic attraction between stator and rotor poles. In this framework, current is applied to a stator phase only while its inductance is increasing and turned off when the inductance begins to decrease, ensuring that only positive torque is produced [1]. However, implementing this type of control is often challenging, as it theoretically requires pulsed phase currents. To simplify the control of VRMs, torque generation can alternatively be understood through the interaction between the stator and rotor magnetic fields. This interpretation leads to the use of unipolar sinusoidal phase currents, which contain both AC and DC components [20], [21]. Accordingly, in this paper, we assume unipolar sinusoidal phase currents of the form (AC with DC offset):

$$i_k = m\,\frac{i_{\mathrm{dc}}}{n}\cos\left(\theta+\theta_i-(k-1)\,\frac{2\pi}{n}\right)+\frac{i_{\mathrm{dc}}}{n}, \qquad (1)$$

where $m \in [0,1]$ is the modulation index, the peak amplitude of the AC component is $m\,\frac{i_{\mathrm{dc}}}{n}$, the DC offset is $\frac{i_{\mathrm{dc}}}{n}$, and θ_i denotes the electrical angle phase shift of the current with respect to the inductance profile that is introduced later. It should be noted that the sum of all phase currents equals the total DC-link current:

$$\sum_{k=1}^{5} i_k = i_{\mathrm{dc}}, \qquad (2)$$

as dictated by Kirchhoff's current law when applied to the VRM circuit shown in **Fig. 1(a)**.

As explained in detail in [10], the proposed uniCSI for VRMs (see **Fig. 1(a)**) controls each switch S_k using a duty cycle d_k to regulate the corresponding phase current as follows:

$$i_k = d_k\, i_{\mathrm{dc}}. \qquad (3)$$

It should be emphasized that this is a form of current modulation, and appropriate overlap between switching intervals must be applied during phase commutation to ensure continuous operation. From (3), the duty cycle can be expressed as:

$$d_k = \frac{i_k}{i_{\mathrm{dc}}} = \frac{m}{n}\cos\left(\theta+\theta_i-(k-1)\,\frac{2\pi}{n}\right)+\frac{1}{n} \qquad (4)$$

Furthermore, the sum of all duty cycles at any instant equals one:

$$d_{\mathrm{tot}} = \sum_{k=1}^{n} d_k = 1. \qquad (5)$$

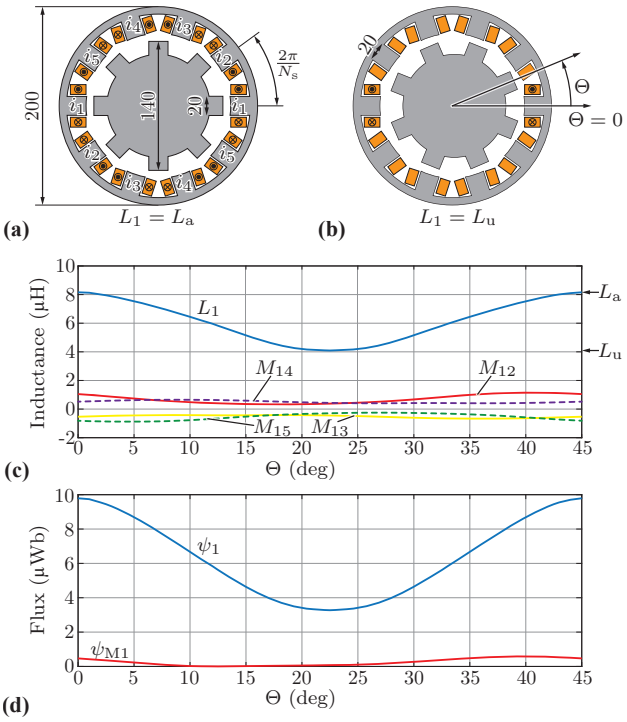

Fig. 2: Five-phase 10/8 VRM example with $N_{\mathrm{s}} = 10$ stator teeth and $N_{\mathrm{r}} = 8$ rotor teeth; all dimensions are in millimeters: **(a)** Phase 1 inductance at its maximum, $L_1 = L_{\mathrm{a}}$, when the rotor teeth are aligned with the stator teeth of phase 1 ($\Theta = 0$). **(b)** Phase 1 inductance at its minimum, $L_1 = L_{\mathrm{u}}$, when the rotor teeth are unaligned with the stator teeth of phase 1 ($\Theta = \frac{\pi}{N_{\mathrm{r}}}$). **(c)** Waveforms of the phase inductance L_1 and mutual inductances $M_{12}, M_{13}, M_{14}, M_{15}$. **(d)** Main flux ψ_1 and mutual flux ψ_{M1}. The waveforms are per meter per turn and obtained from 2D-FEM simulations.

III. VRM Model

To demonstrate the concept of a VRM operating like a series-excited DC machine, we consider an $n = 5$ phase VRM as shown in **Fig. 2**. However, the proposed concept is applicable to VRMs with any number of phases. As highlighted in recent literature [22], five-phase VRMs can offer reduced torque ripple, and thus, lower acoustic noise during operation. In the example configuration, the

stator has $N_\mathrm{s} = 10$ teeth and the rotor has $N_\mathrm{r} = 8$ teeth. The inductance of each stator phase varies between its minimum value L_u, when the stator and rotor teeth are unaligned, and its maximum value L_a, when they are aligned. To analyze how the phase inductance and mutual inductances vary with rotor position, a 2D finite element model (FEM) of the VRM is established using the geometrical parameters shown in **Fig. 2(a,b)**. It should be noted that the geometry is not optimized; its sole purpose is to illustrate the qualitative behavior of the inductance waveforms. **Fig. 2(c)** shows the phase inductance and mutual inductance waveforms as functions of the mechanical rotor angle. The results indicate that the mutual inductances are significantly smaller than the phase inductance. Moreover, due to alternating winding directions (see **Fig. 2(a)**), the mutual inductances take both positive and negative values. Since the motor operates with unipolar phase currents, the total mutual flux contribution to phase 1, defined as $\psi_{\mathrm{M1}} = M_{12}i_2 + M_{13}i_3 + M_{14}i_4 + M_{15}i_5$, is considerably smaller than the main flux contribution from phase 1 itself, $\psi_1 = L_1 i_1$, as illustrated in **Fig. 2(d)**. Therefore, to simplify the analytical derivations in this paper, the effect of mutual coupling will be neglected, i.e., we assume $\psi_{\mathrm{M1}} = 0$. For these calculations, the phase current expression from (1) is used with the parameter values set to $m = 1$, $n = 5$, $i_\mathrm{dc} = 1\,\mathrm{A}$, and $\theta_i = \pi/2$.

In **Fig. 2(b)**, the mechanical rotor angle Θ is indicated. However, for the purposes of our VRM model, the electrical angle θ is more relevant. It is related to the mechanical angle through the number of rotor teeth:

$$\theta = N_\mathrm{r}\Theta. \tag{6}$$

Consequently, the mechanical angular speed Ω and the electrical angular frequency ω are defined as:

$$\Omega = \frac{\mathrm{d}\Theta}{\mathrm{d}t} \qquad \omega = \frac{\mathrm{d}\theta}{\mathrm{d}t}, \tag{7}$$

and are related by the same factor $\omega = N_\mathrm{r}\Omega$.

With all relevant parameters defined, the phase inductance can be expressed as

$$L_k(\theta) = L_\mathrm{u} + (L_\mathrm{a} - L_\mathrm{u})\, f_k(\theta), \tag{8}$$

where $k \in \{1, 2, 3, 4, 5\}$ denotes the phase order and $f_k(\theta)$ is a function that models the variation of inductance between its minimum and maximum values, L_u and L_a. This function typically exhibits a nearly sinusoidal waveform (see FEM simulation results in **Fig. 2(c)**), but for simplicity, it is commonly approximated by a pure sinusoid, which is the approach adopted in this work:

$$f_k(\theta) = \frac{1}{2} + \frac{1}{2}\cos\left(\theta + (k-1)\,\frac{2\pi}{n}\right). \tag{9}$$

Furthermore, magnetic saturation effects are neglected in our model. This simplification is justified since the focus of this work is not on detailed magnetic design or geometric optimization, but rather on demonstrating the operating principle of a VRM driven to behave like a series-excited DC machine.

The voltage equation for each phase is given by

$$u_k = R\, i_k + \frac{\mathrm{d}\psi_k}{\mathrm{d}t}, \tag{10}$$

where the flux linkage per phase is defined as

$$\psi_k(\theta) = L_k(\theta)\, i_k(\theta). \tag{11}$$

Due to the angle dependence of the flux linkage, the time derivative in (10) becomes

$$\frac{\mathrm{d}\psi_k}{\mathrm{d}t} = \frac{\mathrm{d}\psi_k}{\mathrm{d}\theta} \cdot \frac{\mathrm{d}\theta}{\mathrm{d}t} = \frac{\mathrm{d}\psi_k}{\mathrm{d}\theta}\,\omega. \tag{12}$$

Substituting (11) into the above expression yields

$$\frac{\mathrm{d}\psi_k}{\mathrm{d}t} = \frac{\mathrm{d}(L_k i_k)}{\mathrm{d}\theta}\,\omega = i_k \frac{\mathrm{d}L_k}{\mathrm{d}\theta}\,\omega + L_k \frac{\mathrm{d}i_k}{\mathrm{d}\theta}\,\omega. \tag{13}$$

Therefore, the phase voltage expression in (10) becomes

$$u_k = R\, i_k + i_k \frac{\mathrm{d}L_k}{\mathrm{d}\theta}\,\omega + L_k \frac{\mathrm{d}i_k}{\mathrm{d}\theta}\,\omega. \tag{14}$$

To simplify the notation throughout this work, we assume that all quantities are functions of the electrical angle θ, but omit the explicit dependence for brevity. That is, we write $L_k = L_k(\theta)$, $\psi_k = \psi_k(\theta)$, $i_k = i_k(\theta)$, and apply the same convention to all further expressions.

IV. DC-Side Speed-Torque Characteristic

The proposed uniCSI for VRMs from [10] that is shown in **Fig. 1(a)**, algebraically links the VRM phase currents to the DC-link current, see (3). Since the phase currents directly determine the torque produced by the VRM, the uniCSI enables torque control by regulating the DC-link current, provided that the desired modulation index m is fixed (a similar approach was presented in [23], [24] for CSI-supplied permanent magnet synchronous machines). Accordingly, this section focuses on deriving an equivalent speed-torque characteristic using parameters defined on the DC side of the uniCSI.

The derivation of the DC-side equivalent speed-torque characteristic begins with establishing a DC-side equivalent model of the VRM. This is achieved through a power balance approach, where the input power on the DC side must equal the sum of the powers consumed by each individual phase (see **Fig. 1(a)**):

$$\langle u_\mathrm{a} \rangle\, i_\mathrm{dc} = \sum_{k=1}^{5} u_k\, i_k. \tag{15}$$

Here, u_a denotes the DC (armature) voltage and $\langle\cdot\rangle$ represents the average over one switching period, as shown in **Fig. 1(a)**. In practice, this voltage is generated by a switched power converter, such as a half-bridge or full-bridge, so we use its averaged value over one switching period, denoted as $\langle u_\mathrm{a} \rangle$, in the power balance equation (15). The VRM phase voltage u_k and current i_k are defined in (10) and (1), respectively. In this analysis, the influence of the filter capacitors C_f is neglected, as their typical low capacitance is designed only to filter high-frequency current components. Therefore, they have a negligible impact on the fundamental frequency behavior,

which is the basis for the DC-equivalent circuit derivation, see also [23].

If we consider only the voltage drop across the VRM winding resistance R in the phase voltage expression (10), and apply the power balance principle from (15), we obtain the following relation:

$$\langle u_\mathrm{a} \rangle \, i_\mathrm{dc} = R \sum_{k=1}^{5} i_k^2 = \underbrace{\frac{m^2+2}{10} R}_{=R_\mathrm{dc}} \, i_\mathrm{dc}^2, \tag{16}$$

from which the equivalent DC-side resistance can be identified as $R_\mathrm{dc} = \frac{(m^2+2)}{10} R$.

The second voltage component in (10) arises from the change in flux linkage, which is further expanded in (14). The flux per phase, given by $\psi_k = L_k i_k$, depends on both the inductance and the phase current, which vary with time. To capture the most general case, we assume that both the modulation index and the DC-link current, defining i_k in (1), are time-dependent, i.e., $m = m(t)$ and $i_\mathrm{dc} = i_\mathrm{dc}(t)$. Under this assumption, the power balance leads to the following expression:

$$\begin{aligned} \langle u_\mathrm{a} \rangle \, i_\mathrm{dc} &= \sum_{k=1}^{5} \frac{\mathrm{d}\psi_k}{\mathrm{d}t} \, i_k \\ &= \left(L_\mathrm{dc} \frac{\mathrm{d}i_\mathrm{dc}}{\mathrm{d}t} + R_\mathrm{x} \, i_\mathrm{dc} + R_\tau \, i_\mathrm{dc} \right) i_\mathrm{dc} \end{aligned} \tag{17}$$

where L_dc, R_x, and R_τ are DC-side equivalent parameters that model the effect of the time-varying phase inductance L_k as the VRM rotates. The equivalent DC inductance is defined as:

$$L_\mathrm{dc} = \frac{(m^2+2) L_\Sigma + 2m \cos\theta_i \, L_\Delta}{20}, \tag{18}$$

where $L_\Sigma = L_\mathrm{a} + L_\mathrm{u}$ and $L_\Delta = L_\mathrm{a} - L_\mathrm{u}$. The dynamic resistance R_x accounts for the change in magnetic energy due to variations in the modulation index. It is only present when $m(t)$ varies and may take positive or negative values:

$$R_\mathrm{x} = \frac{m \, L_\Sigma + \cos\theta_i \, L_\Delta}{20} \frac{\mathrm{d}m}{\mathrm{d}t}. \tag{19}$$

The electromechanical torque resistance R_τ represents the power component transferred to the VRM shaft and converted into mechanical power:

$$R_\tau(\Omega) = \frac{m \sin\theta_i \, L_\Delta}{20} \, N_\mathrm{r} \Omega. \tag{20}$$

These components together define the DC-side equivalent circuit of the uniCSI-supplied VRM, as shown in **Fig. 3(a)**.

The most important element in the DC-side equivalent circuit shown in **Fig. 3(a)**, in the context of deriving the speed-torque characteristic of the VRM, is the electromechanical torque resistance R_τ. The power developed over this resistance, given by $R_\tau \, i_\mathrm{dc}^2$, corresponds to the mechanical power $T\Omega$ delivered to the VRM shaft, where T is the electromagnetic torque and Ω is the mechanical angular speed. From the power balance, we obtain the following relationship:

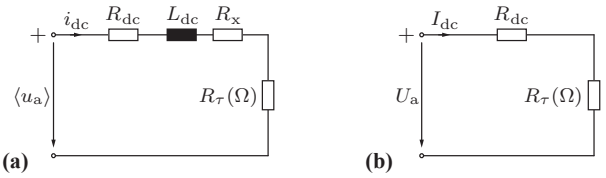

Fig. 3: VRMs DC-side equivalent circuit: **(a)** dynamic circuit, and **(b)** steady-state circuit used for derivation of the speed-torque characteristic.

$$R_\tau \, i_\mathrm{dc}^2 = T \, \Omega = T \, \frac{\omega}{N_\mathrm{r}}, \tag{21}$$

which allows us to express the electromagnetic torque as a function of the DC-link current:

$$T = \frac{2}{5} \, m \sin\theta_i \, L_\Delta \, i_\mathrm{dc}^2, \tag{22}$$

where we assumed $N_\mathrm{r} = 8$. From (22), we can define a torque constant

$$k_\mathrm{T} = \frac{2}{5} \, m \sin\theta_i \, L_\Delta, \tag{23}$$

so that the torque expression is $T = k_\mathrm{T} i_\mathrm{dc}^2$. In addition, the electromechanical torque resistance from (20) becomes equal to $R_\tau(\Omega) = k_\mathrm{T}\Omega$.

The speed-torque characteristic is derived under steady-state conditions. Accordingly, assuming steady-state operation, the dynamic VRM equivalent circuit shown in **Fig. 3(a)** reduces to the steady-state representation depicted in **Fig. 3(b)**. In this context, voltages and currents are denoted with capital letters (U_a and I_dc) to indicate steady-state values.

The speed-torque relationship is obtained starting from the steady-state voltage equation:

$$U_\mathrm{a} = R_\mathrm{dc} \, I_\mathrm{dc} + R_\tau(\Omega) \, I_\mathrm{dc}. \tag{24}$$

Substituting $I_\mathrm{dc} = \sqrt{T/k_\mathrm{T}}$ and $R_\tau(\Omega) = k_\mathrm{T} \, \Omega$ into (24), and solving for the mechanical speed Ω, we obtain:

$$\Omega(T) = \frac{U_\mathrm{a}}{\sqrt{k_\mathrm{T} \, T}} - \frac{R_\mathrm{dc}}{k_\mathrm{T}}, \tag{25}$$

which represents the desired steady-state speed-torque characteristic of the VRM.

The derived speed-torque characteristic closely resembles that of a series-excited DC machine, thereby making the control of the uniCSI-supplied VRM drive system from the DC side functionally equivalent to that of a series-excited DC machine. Moreover, the characteristic in (25) can be tuned by adjusting the modulation index m, since the torque constant k_T depends on m; see (23). The influence of k_T is illustrated in **Fig. 4(a)**, where the speed-torque characteristic (25) is plotted for different values of m. The remaining parameters are listed in **Tab. I**. The rotational speed is presented in revolutions per minute (rpm) rather than radians per second, using the conversion $n_\mathrm{mech} = \Omega \cdot \frac{30}{\pi}$. It should be noted that this extension of the speed-torque range by reducing m comes at the cost

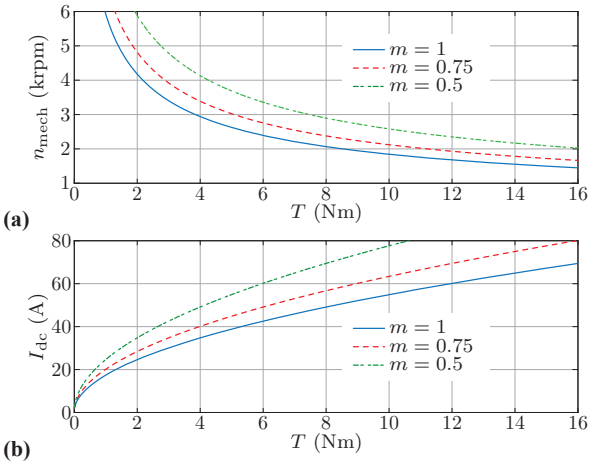

Fig. 4: Impact of the modulation index m on the speed-torque characteristic: **(a)** speed versus torque curves, and **(b)** DC-link current versus torque curves.

Parameter	Symbol	Value
DC-link voltage	$\langle u_{\mathrm{a}} \rangle = U_{\mathrm{a}}$	36 V
Current angle	θ_i	$\pi/2$
Inductance difference	L_Δ	8.3 mH
DC-side resistance	R_{dc}	0.015 Ω

TABLE I: Speed-Torque Characteristic Parameters.

of increased DC-link current, as shown in **Fig. 4(b)**. This is expected: reducing m decreases the torque constant k_{T}, which in turn requires a higher DC-link current to generate the same torque.

V. Maximizing Torque per Current

As discussed in the previous section and illustrated in **Fig. 4**, the equivalent DC-side speed-torque characteristic of the VRM can be adjusted through the CSI modulation index m and the current phase angle θ_i. In the remainder of this paper, we fix these values to maximize the torque-per-ampere ratio. From (22) and (23), it follows that the maximum torque per unit current is achieved when

$$m = M = 1 \qquad \theta_i = \theta_I = \frac{\pi}{2}, \tag{26}$$

where the capital letters M and θ_I are used to denote these fixed, optimal values.

In this scenario, the DC-side equivalent parameters simplify significantly. The DC-side resistance from (16) reduces to

$$R_{\mathrm{dc}} = \frac{3}{10} R, \tag{27}$$

and the DC-side inductance from (18) reduces to

$$L_{\mathrm{dc}} = \frac{3}{20} L_\Sigma. \tag{28}$$

Since the modulation index is constant, the dynamic resistance from (19) becomes zero, i.e., $R_{\mathrm{x}} = 0$. The electromechanical torque resistance from (20) simplifies to

$$R_\tau(\Omega) = \frac{2}{5} L_\Delta \, \Omega. \tag{29}$$

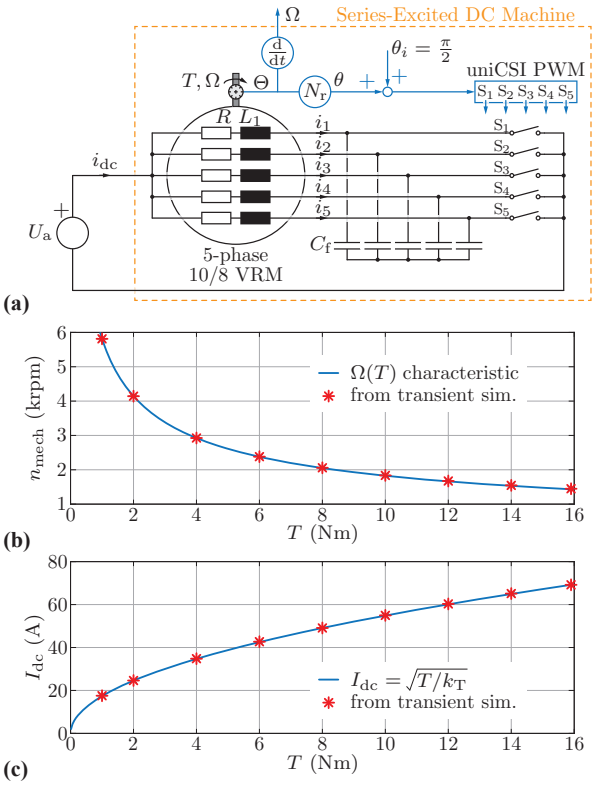

Fig. 5: Verification of the speed-torque characteristic: **(a)** Transient time-domain simulation schematic with a constant voltage of $U_{\mathrm{a}} = 36$ V. **(b)** Speed-torque characteristic (25), where red dots indicate the steady-state speed reached in the transient time-domain simulation. **(c)** DC-link current vs. torque characteristic, illustrating the quadratic dependence of torque on the DC-link current.

Finally, the torque constant expression simplifies to

$$k_{\mathrm{T}} = \frac{2}{5} L_\Delta. \tag{30}$$

VI. Simulation Results

The simulation results are obtained using time-domain simulations in PLECS, employing a 10/8 VRM model that implements the same analytical model described in this paper, as detailed in **Sec. III**.

A. Speed-Torque Characteristic

The speed-torque characteristic is validated through simulations of the schematic shown in **Fig. 5(a)**. The CSI operates in open-loop mode. Its duty cycles are computed using (4), where both the modulation index and the DC-link current angle are held constant, as specified in (26). As demonstrated in **Sec. IV**, such a uniCSI-supplied VRM exhibits DC-side behavior equivalent to that of a series-excited DC machine. Consequently, the VRM can be directly connected to a constant voltage source, enabling the validation of the speed-torque characteristic (25). The resulting data is shown in **Fig. 5(b)**.

Each star-shaped point corresponds to a separate transient simulation that settles at a steady-state speed. This final speed is recorded and plotted. The mechanical load torque applied to the VRM is varied between 1 Nm and

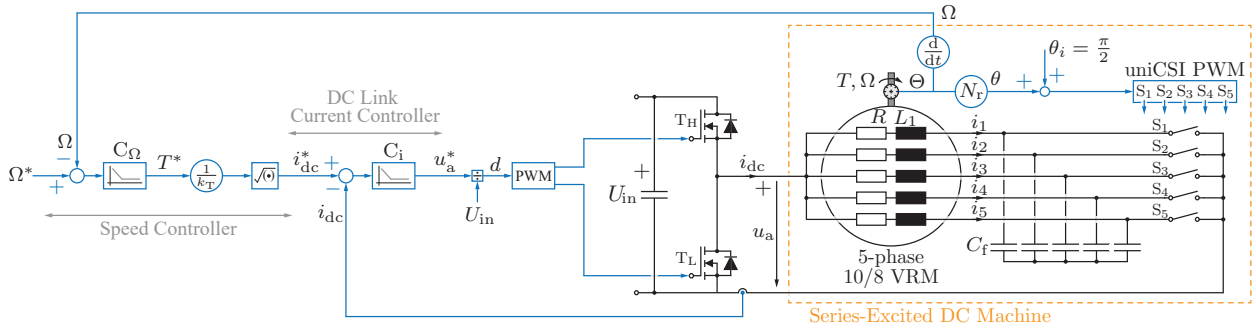

Fig. 6: Speed control block diagram, illustrating the regulation of VRM speed and torque through the DC-link current via the input buck converter. As a result, the uniCSI-supplied VRM drive exhibits a behavior similar to that of a series-excited DC machine from the user's perspective. The uniCSI operates with PWM modulation and open-loop control, relying solely on the VRM's rotor angle information.

16 Nm. The continuous line that closely follows these simulation points corresponds to the theoretical curve described by (25). Numerical parameters used in the simulation are provided in **Tab. I**. A match between the analytical speed–torque characteristic (25) and the simulation results is achieved, thereby validating the derived expression (25) as well as confirming the quadratic relationship between torque and DC-link current, see **Fig. 5(b,c)**.

B. Speed-Controlled Drive System

As shown in the previous subsection, once the uniCSI duty cycle angle is synchronized with the VRM's shaft position and shifted by $\pi/2$ electrical, the uniCSI-supplied VRM drive behaves, at its DC-side terminals, like a series-excited DC machine. This equivalence is demonstrated by the results shown in **Fig. 5**. Consequently, from the user's perspective, the uniCSI-supplied VRM can be treated entirely as a series-excited DC machine, without the need to manage uniCSI control or modulation, as it operates in an open-loop manner. This simplifies torque control of the VRM, which can now be achieved by regulating the DC-link current. This concept enables, for example, the implementation of a speed control system as illustrated in **Fig. 6**.

Time-domain simulation of the proposed drive system shown in **Fig. 6** is carried out, and the results are presented in **Fig. 7**. The numerical values of the parameters used in the simulation are provided in **Tab. II**. The results confirm the expected direct correspondence between the DC-link current and the VRM torque. The maximum torque of the VRM, 32 N m (twice the nominal value), is achieved during the acceleration phase of the drive system. This corresponds to a DC-link current of $\sqrt{T/k_{\mathrm{T}}} = 98.2\,\mathrm{A}$. Once the final speed reference is reached, the torque settles to its nominal value of 16 N m, and accordingly, the DC-link current decreases to 69.4 A.

The duty cycles d_1, d_2, d_3, d_4, d_5 are computed according to (4) without the need for any control algorithm or user intervention; only rotor angle information from an encoder is required, thereby fully abstracting the uniCSI operation from the user's perspective. This simplicity

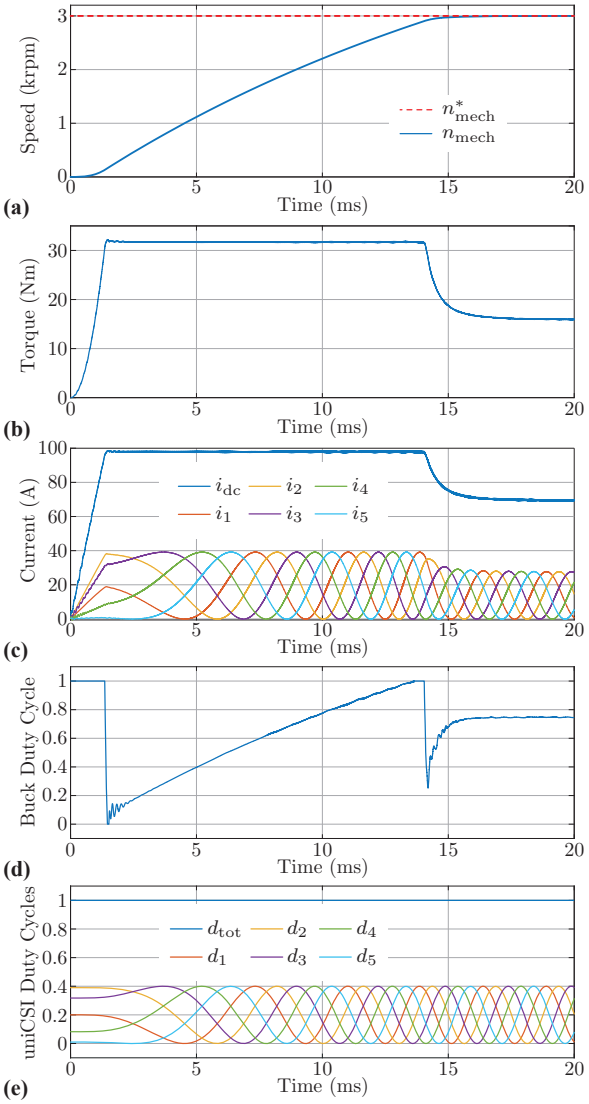

Fig. 7: Transient simulation results: **(a)** Mechanical speed, **(b)** VRM torque, **(c)** DC-link and VRM phase currents, **(d)** Input buck converter duty cycle, and **(e)** uniCSI duty cycles along with their total sum, ensuring $d_{\mathrm{tot}} = 1$. The uniCSI modulation is implemented according to [25].

Parameter	Symbol	Value
Buck		
Input voltage	U_{in}	100 V
Switching frequency	$f_{\mathrm{sw,b}}$	300 kHz
CSI		
Output capacitance	C_{f}	0.2 µF
Switching frequency	f_{sw}	300 kHz
Modulaiton index	M	1
Current angle	θ_I	$\pi/2$
VRM		
Phase resistance	R	0.05 Ω
Unaligned inductance	L_{u}	0.5 mH
Aligned inductance	L_{a}	8.8 mH
Number of stator teeth	N_{s}	10
Number of rotor teeth	N_{r}	8
Moment of inertia	J	0.001 kgm^2
Nominal mech. power	P_{mech}	5 kW
Nominal mech. speed	n_{mech}	3000 rpm
DC-side		
DC-side resistance	R_{dc}	0.015 Ω
DC-side inductance	L_{dc}	1.395 mH
Torque constant	k_{T}	3.32 mN m A^{-2}
Controller gains		
$\mathrm{C_i}$ closed-loop bandwidth	f_{cc}	5 kHz
$\mathrm{C_i}$ proportional gain	K_{pc}	43.82 V/A
$\mathrm{C_i}$ integral gain	K_{ic}	33 143 V/(As)
C_Ω cross-over frequency	f_{cs}	0.5 kHz
C_Ω proportional gain	K_{ps}	3.14 s N m
C_Ω integral gain	K_{is}	1974 N m

TABLE II: Simulation Parameters.

enables the uniCSI and VRM to be combined into a single, compact unit, as illustrated in **Fig. 8**.

It is essential to emphasize that, due to the VRM's open-end winding configuration, the integrated uniCSI does not require a dedicated DC-link inductor and operates with only one switch per phase. This approach allows the VRM and its tailored uniCSI to be co-designed and integrated, eliminating the typical complexity and ambiguity associated with selecting an appropriate inverter for VRMs. In practical terms, users of the proposed drive system interface with a universal motor (series-excited DC machine) that can be supplied via a standard half- or full-bridge converter, depending on the specific application requirements.

VII. Conclusion

This paper proposes an unipolar current source inverter (uniCSI)-supplied variable reluctance motor (VRM) drive system. The uniCSI used is a recently introduced topology that requires only half the number of semiconductors compared to conventional CSIs, specifically, one switch per VRM phase. Furthermore, thanks to the open-end winding configuration of the VRM, the proposed uniCSI does not require a dedicated DC-link inductor, as the VRM's own inductance serves this role effectively from the DC-side perspective.

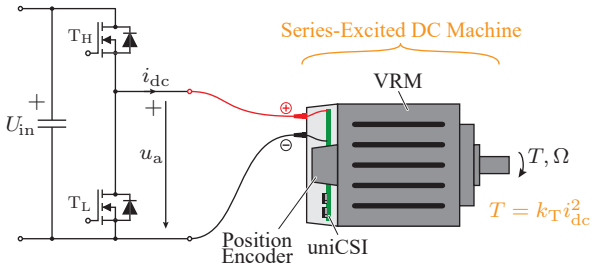

Fig. 8: Proposed uniCSI-supplied VRM drive with the uniCSI and VRM integrated into a single housing, enabling straightforward usage as a series-excited DC machine,i.e., a universal motor from the user's perspective.

This inverter-motor combination enables open-loop operation of the uniCSI using only rotor position feedback. As a result, torque control is achieved solely through regulation of the DC-link current, making the system extremely simple to operate and easy to integrate into a wide range of applications. We have shown that the proposed uniCSI-supplied VRM exhibits a quadratic relationship between torque and DC-link current, analogous to the behavior of a series-excited DC machine. Additionally, we demonstrated how speed and torque can be controlled entirely from the DC side, abstracting away the uniCSI from the user's perspective.

Finally, we outlined our future direction, which focuses on physically integrating the uniCSI and VRM into a single unit with only two external terminals, positive and negative DC connections, allowing the entire system to function as a plug-and-play universal motor.

References

[1] W. Ray and R. Davis, "Inverter drive for doubly salient reluctance motor: its fundamental behaviour, linear analysis and cost implications," *IEE Journal on Electric Power Applications*, vol. 2, no. 6, pp. 185–193, 1979.

[2] P. Lawrenson, J. Stephenson, P. Blenkinsop, J. Corda, and N. Fulton, "Variable-speed switched reluctance motors," *IEE Proceedings B (Electric Power Applications)*, vol. 127, no. 4, pp. 253–265, 1980.

[3] T. J. Miller, "Converter volt-ampere requirements of the switched reluctance motor drive," *IEEE Transactions on Industry Applications*, no. 5, pp. 1136–1144, 1985.

[4] A. Clothier and B. Mecrow, "Inverter topologies and current sensing methods for short pitched and fully pitched winding SR motors," in *Proc. of the Applied Power Electronics Conference and Exposition (APEC 99)*, vol. 1. Texas, USA: IEEE, 1999, pp. 416–423.

[5] Y. Tang, "Switched reluctance motor with fractionally pitched windings and bipolar currents," in *Proc. of the IEEE Industry Applications Conference (IAS 98)*, vol. 1. Missouri, USA: IEEE, 1998, pp. 351–358.

[6] H. Le-Huy, P. Viarouge, and B. Francoeur, "Unipolar converters for switched reluctance motors," in *Proc. of the IEEE Industry Applications Society Annual Meeting*. California, USA: IEEE, 1989, pp. 551–560.

[7] C. Pollock and B. W. Williams, "Power convertor circuits for switched reluctance motors with the minimum number of switches," *IEE Proceedings B (Electric Power Applications)*, vol. 137, no. 6, pp. 373–384, November 1990.

[8] S. Vukosavic and V. R. Stefanovic, "SRM inverter topologies: A comparative evaluation," *IEEE Transactions on industry applications*, vol. 27, no. 6, pp. 1034–1047, 1991.

[9] Ž. Grbo, S. Vukosavić, and E. Levi, "A novel power inverter for switched reluctance motor drives," *Facta universitatis-series: Electronics and Energetics*, vol. 18, no. 3, pp. 453–465, 2005.

[10] T. Ohno, M. Haider, and S. Mirić, "A switch-per-phase PWM current source inverter topology for switched reluctance motor drives," in *VDE Tagung Elektromechanische Antriebssysteme*. VDE, 2025, to appear.

[11] S. H.-Y. Li, F. Liang, Y. Zhao, and T. A. Lipo, "A doubly salient doubly excited variable reluctance motor," *IEEE transactions on industry applications*, vol. 31, no. 1, pp. 99–106, 1995.

[12] T. Fukami, Y. Matsuura, K. Shima, M. Momiyama, and M. Kawamura, "A multipole synchronous machine with nonoverlapping concentrated armature and field windings on the stator," *IEEE Transactions on Industrial Electronics*, vol. 59, no. 6, pp. 2583–2591, 2011.

[13] Y. Fan, K. Chau, and S. Niu, "Development of a new brushless doubly fed doubly salient machine for wind power generation," *IEEE Transactions on Magnetics*, vol. 42, no. 10, pp. 3455–3457, 2006.

[14] Z. Azar and Z. Zhu, "Performance analysis of synchronous reluctance machines having nonoverlapping concentrated winding and sinusoidal bipolar with DC bias excitation," *IEEE Transactions on Industry Applications*, vol. 50, no. 5, pp. 3346–3356, 2014.

[15] X. Liu and Z. Zhu, "Stator/rotor pole combinations and winding configurations of variable flux reluctance machines," *IEEE Transactions on Industry Applications*, vol. 50, no. 6, pp. 3675–3684, 2014.

[16] S. Jia, D. Liang, W. Kong, R. Qu, Z. Yu, D. Li, and P. Kou, "A high torque density concentrated winding vernier reluctance machine with dc-biased current," *IEEE Transactions on Magnetics*, vol. 54, no. 11, pp. 1–5, 2018.

[17] W. Kong, D. Jiang, R. Qu, Z. Yu, S. Jia, and L. Jing, "Drive for DC-biased sinusoidal current vernier reluctance motors with reduced power electronics devices," in *Proc. of the IEEE International Electric Machines and Drives Conference (IEMDC)*. Florida, USA: IEEE, 2017, pp. 1–6.

[18] A. Li, D. Jiang, W. Kong, and R. Qu, "Four-leg converter for reluctance machine with DC-biased sinusoidal winding current," *IEEE transactions on power electronics*, vol. 34, no. 5, pp. 4569–4580, 2018.

[19] R. Kojima, K. Naruse, and N. Hoshi, "Characteristics of switched reluctance motor driven by four-leg inverter applied with PWM control," in *Proc. of the IEEE Industrial Electronics Society (IECON 2023)*. Singapore: IEEE, 2023, pp. 1–6.

[20] K. Kawarazaki, R. Kojima, and N. Hoshi, "Vector control of srm based on general rotating coordinate system synchronized with electrical rotor angle," in *2023 12th International Conference on Renewable Energy Research and Applications (ICRERA)*. IEEE, 2023, pp. 231–236.

[21] N. Nakao and K. Akatsu, "Vector control specialized for switched reluctance motor drives," *Electrical Engineering in Japan*, vol. 194, no. 2, pp. 24–36, 2016.

[22] T. Kumagai, J.-i. Itoh, and K. Kusaka, "Reduction method of torque ripple, dc current ripple, and radial force ripple with control flexibility of five-phase srm," in *2020 IEEE Energy Conversion Congress and Exposition (ECCE)*. IEEE, 2020, pp. 4703–4708.

[23] S. Mirić, P. Pejović, T. Ohno, and M. Haider, "Current source inverter drive system with equivalent DC-machine control characteristics," in *Proc. of 27th International Conference on Electrical Machines and Systems (ICEMS 2024)*. Fukuoka, Japan: IEEJ, 2024.

[24] S. Mirić, P. Pejović, T. Ohno, and M. Haider, "Current source inverter-supplied pmsm drive system for dc machine-like operation," *IEEJ Journal of Industry Applications*, p. 25000231, 2025.

[25] P. Pejović, T. Ohno, U. Borović, and S. Mirić, "Pulse width modulation for current source inverters with arbitrary number of phases," *Scientific Reports*, vol. 15, no. 1, p. 8744, 2025.